

## Development of Heat Input Estimation Technique for Simulation of Shell Forming by Line-Heating

N. Osawa<sup>1</sup>, K. Hashimoto<sup>1</sup>, J. Sawamura<sup>1</sup>, J. Kikuchi<sup>2</sup>, Y. Deguchi<sup>2</sup> and T. Yamaura<sup>2</sup>

**Abstract:** A new hypothesis regarding heat transmission during line heating is proposed. It states that the distribution of the temperature of the gas adjacent to the plate,  $T_G$ , and the overall local heat transfer coefficient,  $\alpha$ , depend only on the distance from the torch. An identification technique for  $T_G$  and  $\alpha$  is developed. The validity of the employed hypothesis and the proposed technique is demonstrated by comparing the measured and identified  $T_G$  during a spot heating test. The plate temperature calculated by direct heat conduction analysis closely approximates the one measured for the spot and line heating tests, when  $T_G$  and  $\alpha$  identified from the spot heating test are used as the thermal boundary conditions. This indicates that heat transmission can be estimated for any desired plate shape, dimension and torch movement history, based solely on the spot heating test results.

**Keyword:** Heat flux, Heat transfer, Inverse heat conduction analysis, Laser induced fluorescence technique, Temperature estimation, Line heating.

### 1 Introduction

Flame line heating is an effective method for forming flat steel plates into three-dimensional shapes for ships and other structures. However, this technique requires skilled workers who are now in short supply. Hence the urgent need to automate this process.

The problem of flame forming of metal plate can be separated into two sub-problems: the heat transmission problem and the elasto-plastic defor-

mation problem. In fact, the solution of the first problem is a prerequisite to approaching the second one.

Some reports on the heat transmission problem during line heating have been published to date. Moshaiov and Latorre (1985) studied the temperature distribution of a plate using a distributed heat source moving along the plate surface. Tsuji and Okumura (1988) found that the heat flux distribution could be expressed approximately by the superposition of two Gaussian distributions. Terasaki, Kitamura and Nakai (1999) proposed a predictive equation for the thermal cycle during the line heating process. Jang, Seo and Ko (1997) proposed a heat flux estimation method based on the inherent strain concept, while Yu, Anderson, Maekawa and Patrikalakis (2001) developed a semi-analytically determined thermal model which incorporates the effects of heat loss and a distributed moving heat source.

Very slow torch speed heating and repetitive heating are frequently employed in the final finishing stage of the plate forming process. An accurate temperature calculation technique for these heating procedures has to be established to accomplish the automation of the line heating process.

In the conventional studies listed above, the heat flux distribution around the torch is assumed to remain unchanged with time. This approximation is not sufficient for very slow torch speed and repetitive heating cases. In these cases, the plate face temperature directly below the torch rises substantially over time. This results in a decrease of heat transfer, which makes the heat flux change with time.

Conventional theories cannot be applied to these cases, so it is necessary to develop a new theory suitable for a wide range of applications, on the

<sup>1</sup>Dept. of Naval Architecture and Ocean Engineering, Graduate School of Engineering, Osaka University, Osaka, Japan.

<sup>2</sup>Mitsubishi Heavy Industries Co. Ltd., Nagasaki, Japan.

basis of the true nature of heat transmission between the flame and the plate.

The change in the heat flux can be calculated by thermal fluid and heat transfer simulations. Sawamura, Tomita, Osawa and Hashimoto (2002) developed a combustion model suited to the thermal fluid simulation of line heating process, and showed that the measured and estimated gas temperature agreed well. Shin and Woo (2003) proposed a numerical procedure which comprised a non-combustion thermal fluid analysis and an iterative heat conduction analysis to estimate the heat transfer rate during a spot heating test. The numerical thermal fluid simulation needed in these approaches takes a very long time, and there may be cases where the calculation lacks robustness. It is necessary to develop an alternative method which does not need thermal fluid simulations.

## 2 Estimation of Heat Transmission between the Combustion Flame and the Plate during Spot Heating

### 2.1 Changing nature of the gas temperature field during spot heating

Tomita, Osawa, Hashimoto, Shinkai, Sawamura and Matsuoka (2001) measured in detail the transient 3-dimensional gas temperature field within the combustion flame during spot heating tests by a high performance laser induced fluorescence (LIF) measurement system. LIF is one of the most practical laser diagnostics in combustion analysis (Eckbreth (1988)).

They found that the temperature distribution remained unchanged with time regardless of a substantial temperature rise of the plate face. From this, one can hypothesize that the thermal-flow field of the heating gas becomes stable in an extremely short time, and remains unchanged during spot heating. This means that the temperature of the gas adjacent to the plate (strictly speaking, the temperature at the point adjacent to the boundary layer),  $T_G$ , can be considered to remain nearly unchanged with time.

The above result also leads to the assumption that the change in the thermal-flow field within the boundary layer is small, and that in this case the

local heat transfer coefficient is nearly constant.

Heat transmission between the gas flame and the plate consists of heat transfer and radiation. For simplicity, let us assume that heat transfer predominates. Given that, one can postulate that the entire heat transmission can be approximated as heat transfer, and the overall local heat transfer coefficient,  $\alpha$ , remains unchanged with time.

From the above discussion, a hypothesis that  $T_G$  and  $\alpha$  are time independent and that they depend only on the distance from the torch can be established. This hypothesis leads to a linear relationship between flux  $q$  and heating face temperature  $T_S$  as

$$q(t;r) = -\alpha(r)T_S(t;r) + \alpha(r)T_G(r), \quad (1)$$

where,  $t$  is time and  $r$  is the distance from the torch.

Time histories of plate back surface temperature,  $T_B(t;r)$ , can be measured during a spot heating test. Time histories of flux and heating face temperature,  $q(t;r)$  and  $T_S(t;r)$  can be estimated by inverse heat conduction (IHC) analysis from the measured  $T_B$ . Using Eq. (1),  $T_G(r)$  and  $\alpha(r)$  can be identified by a linear regression analysis on the relation between  $q(t;r)$  and  $T_S(t;r)$ . Heat transmission and plate temperature during spot heating can be calculated when we analyze heat transfer and heat conduction using the identified  $T_G(r)$  and  $\alpha(r)$ . Hereafter, we call  $T_G(r)$  and  $\alpha(r)$  "the heat input parameters".

### 2.2 Identification of the heat flux during spot heating

Let us imagine that the spot heating test is performed using a thin circular steel disk, which is heated by a gas torch fixed at the center. The heat flux on the heating face of the disk is both space- and time-variable. The distribution of the flux can be identified by IHC analysis. There have been varied approaches to IHC problem (e.g. Chang, Liu and Chang (2005), Ling and Atluri (2006), Liu (2006), Liu, Liu and Hong (2007)). In this study, sequential function specification scheme is employed. The spatial variation of  $q$  at time  $t$  is

described by a Fourier cosine series as

$$q(t; r) = \sum_{k=1}^K Q_k(t) \cos(k\pi r/2r_0) + Q_0(t). \quad (2)$$

We examine the quantities at discrete time,  $t_i$  ( $i = 1, 2, \dots$ ), and back surface temperature histories are measured at points  $S_I$  ( $I = 1, \dots, N$ ).  $Y_I^i$  is the back surface temperature at location  $S_I$  and time  $t_i$ , and  $Q_k^i$  ( $k = 0, \dots, K$ ;  $i = 1, 2, \dots$ ) is the value of  $Q_k$  in Eq. (2) at time  $t_i$ . Beck, Blackwell and Clair (1985) showed that  $Q_k^i$  can be identified by the following procedure.

$T_{(0)I}^{M+i}$  ( $i = 1, \dots, m$ ) is the calculated back surface temperature at location  $S_I$  and time  $t_{M+i}$  for the case where all  $Q_k$  ( $k = 0, 1, \dots, K$ ) become zero after  $t_M$ . The first derivatives of back surface temperatures with respect to  $Q_k$  ( $k = 0, 1, \dots, K$ ) are called sensitivity coefficients.

The sensitivity coefficient for the back surface temperature at location  $S_I$  and time  $t_{M+i+r}$ , with respect to  $Q_J$  is represented by  $A_{IJ}^{(r)}$ .  $A_{IJ}^{(r)}$  can be calculated by substituting  $T_{(0)I}^{M+r}$  from the back surface temperature at location  $S_I$  and time  $t_{M+r}$  for the case where  $Q_J^M = 1$  and all other flux components are zero.

$Q_k$  at time  $t_{M+i-1}$  can be identified by the equation below:

$$\{Q\} = ([X]^T [X] + \lambda [H]^T [H])^{-1} [X]^T (\{Y\} - \{T_{(0)}\}), \quad (3)$$

where,  $\{q\}$ ,  $\{Y\}$  and  $\{T\}$  are,

$$\begin{aligned} \{Q\} &= [Q_0^M, \dots, Q_K^M, \dots, Q_0^{M+m-1}, \dots, Q_K^{M+m-1}]^T \\ \{Y\} &= [Y_1^{M+1}, \dots, Y_N^{M+1}, \dots, Y_1^{M+m}, \dots, Y_N^{M+m}]^T \\ \{T_{(0)}\} &= [T_{(0)1}^{M+1}, \dots, T_{(0)N}^{M+1}, \dots, T_{(0)1}^{M+m}, \dots, T_{(0)N}^{M+m}]^T \end{aligned} \quad (4)$$

and the  $(mN) \times (m(K+1))$  matrix  $[X]$  is given as

follows,

$$[X] = \begin{bmatrix} [A_{IJ}^{(0)}] & [0] & \cdots & [0] \\ [A_{IJ}^{(1)}] & [A_{IJ}^{(0)}] & [0] & \vdots \\ \vdots & \vdots & \ddots & [0] \\ [A_{IJ}^{(m-1)}] & [A_{IJ}^{(m-2)}] & \cdots & [A_{IJ}^{(0)}] \end{bmatrix} \quad (5)$$

$m$  in Eq. (5) is the number of the future times used in the calculation.

The  $(m(K+1)) \times (m(K+1))$  matrix  $[H]$  is the regularization matrix.  $\lambda$  is the regularization parameter.  $[H]$  is chosen so that it controls the fluctuation of the time-derivative of  $Q_k$ , and it is given by

$$[H] = \begin{bmatrix} [i_2] & -2[i_2] & [i_2] & & [0] \\ & \ddots & \ddots & \ddots & \\ & & [i_2] & -2[i_2] & [i_2] \\ & & & [0] & [0] \\ [0] & & & & [0] \end{bmatrix}, \quad (6)$$

where,  $(K+1) \times (K+1)$  matrix  $[i_2]$  is

$$[i_1] = \begin{bmatrix} 1 & & & 0 \\ & \ddots & & \\ & & 1 & \\ & & & 0 \\ 0 & & & & 0 \end{bmatrix}, \quad (7)$$

and  $[0]$  is a  $(K+1) \times (K+1)$  zero matrix.

The values of  $T_{(0)I}^{M+i-1}$  in Eq. (3) and the sensitivity coefficients  $A_{IJ}^{(i)}$  in Eq. (5) can be calculated by direct heat conduction (DHC) analysis. When the temperature distribution in the plate at time  $t_M$  is known,  $T_{(0)I}^{M+i}$  ( $I = 1, \dots, N$ ;  $i = 1, \dots, m$ ) can be calculated by assuming  $Q_J = 0$ . ( $J = 0, \dots, K$ ).  $A_{IJ}^{(i)}$  can be derived from the calculated back surface temperature for the case where  $Q_J = 1.0$  in the duration between  $t_{M+i}$  and  $t_{M+i+1}$  and other flux terms of Eq. (2) are zero. From  $T_{(0)I}^{M+i-1}$  and  $A_{IJ}^{(i)}$  obtained by the procedure above, together with the measured back surface temperature  $Y_I^{M+i}$ , it is possible to identify  $Q_J$  in the duration between  $t_{M+i}$  and  $t_{M+i+1}$ ,  $Q_J^M$  ( $J = 0, \dots, K$ ), by Eq. (3). The temperature distribution at time  $t_{M+1}$  is calculated by DHC analysis using these

identified  $Q_j^M$ . Repeating this operation, both the plate temperature and the flux on the heating face at the time  $t_{M+i}$  ( $i = 1, \dots, m$ ) are calculated.

$q(t;r)$  and  $T_S(t;r)$  in Eq. (1) are derived by the above procedure, and the heat input parameters, the temperature of the gas adjacent to the plate  $T_G(r)$  and local (overall) heat transfer coefficient  $\alpha(r)$ , can be identified.

### 3 Identification of Heat Input Parameters during a Spot Heating Test

#### 3.1 Heating apparatus and steel plate temperature measurement system

A circular mild steel disk of diameter  $d=300\text{mm}$  and 6mm thickness, shown in Figure 1, is arranged horizontally and a torch with a #3000 nozzle is positioned above the disk. The distance between the nozzle and the plate is 20mm. The back surface of the disk is coated with a heat insulating material, and the center of the plate is heated by an oxyacetylene flame. The pressure and the flux are 0.38MPa and 40 l/min for acetylene, and 0.85MPa and 39 l/min for oxygen.

The time histories of the plate back surface temperature are measured by K-type thermoelectric couples with a sheath diameter of 0.1mm welded on the plate back surface. The outputs of thermocouples are recorded on a personal computer every 0.5 sec.

As shown in Figure 1, the points at which the back surface temperature is measured are arranged in a radial direction from the center to a point 104mm away from the center. Hereafter,  $r$  denotes the distance from the center. The intervals of the points are 4mm up to the point at which  $r=40\text{mm}$ , and 8mm for the points at which  $r>40\text{mm}$ . For  $r>0$ , the average of two measurements for the same  $r$  is taken as the representative value. In the experiment, heating ceases within about 5 seconds.

#### 3.2 LIF measurement system

The thermal field within the combustion flame is measured by the LIF system developed by Mitsubishi Heavy Industries, Ltd. (Deguchi, Nakagawa, Ichinose and Inada (2000)). Temperature

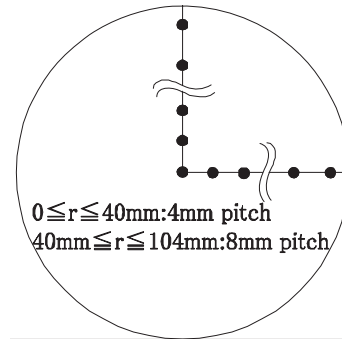


Figure 1: Arrangement of thermocouples for spot heating tests

measurement is undertaken by means of a dual wavelength LIF method using NO.

In the present study, for the fluorescent properties of NO (Reisel, Carter and Laurendeau, 1992), the two excitation wavelengths of 226.8nm ( $P2(4.5) + Q12(4.5) + P2(2.5) + Q12(2.5)$ ) and 224.178nm ( $Q1(38.5) + Q2(39.5)$ ) are selected as being suitable for the 1,500~2,500K central region of the flame temperature range. Figure 2 presents a schematic view of the LIF temperature measurement optical system.

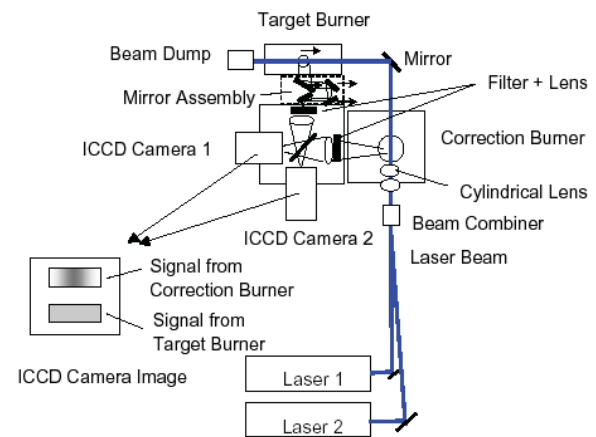


Figure 2: Optical setup of LIF measurement system

A YAG laser-excited dye laser (YAG laser: GCR-250, dye laser: PDL-3, wavelength converter: WEX-3, Spectra Physics, dyes: Rhodamine 590 and Rhodamine 610) is set to the absorption wavelength of NO, and is operated at 10Hz. Laser

light is coaxially aligned using a beam combiner, and is then directed to the intensity distribution correction burner and plate bending burner. Imaging of the fluorescence from each of the flames is detected via mirrors using two ICCD cameras (Flame Star III, LA-VISION). The upper half and lower half images are then merged, and the intensity distribution is measured. The laser apparatus and the image capturing timing are controlled using a delay generator (DG535, SRS). The captured images are then transferred to a computer and flame temperature is calculated.

The LIF measured region is 81.9mm in width and 19.8mm in height, and the distance between the plate face and the bottom of the region is 0.5 mm. The space resolution of the captured image is 0.51 mm $\times$ 0.51mm. In LIF measurement, laser exposure is for 0.4 seconds, and images are captured every 2 seconds. Measurement is initiated immediately prior to the setting of the ignited torch at the designated point.

As in the experimental results obtained by Tomita, Osawa, Hashimoto, Shinkai, Sawamura and Matsuoka (2001) and Deguchi, Yamaura, Kawano, Tsubouchi, Tomita, Osawa, Hashimoto, Shinkai, Sawamura and Sugiyama (2002), it is found that the moving time-average of the measured gas temperature at each point within the flame remains almost unchanged through the spot heating test. That is, the averaged thermal-flow field becomes stable in an extremely short time.

### 3.3 Identification of flux and plate heating face temperature

Though the temperature should be the highest at the center, the measured back surface temperatures at the location  $r=0$ , 4mm are lower than that at  $r=8$ mm. It is supposed that an excessive heat input causes the slowdown of the response of the thermocouples near the center. Because of this, the temperatures at  $r=0$  and 4mm are not used in IHC analysis.

The number of terms of the series  $K$  in Eq. (2) is set to 6.  $r_0$  is set to the radius of the disk,  $d/2$ . The number of the future times  $m$  is set to 4. The regularization parameter  $\lambda$  in Eq. (3) is chosen so that the Euclid norm of the regularization matrix

is 1/10 as large as that of the sensitivity term.

$T_{(0)I}^{M+i-1}$  in Eq. (3) and  $A_{IJ}^{(i)}$  in Eq. (5) are calculated by axisymmetric finite element (FE) DHC analysis. The temperature dependencies of the material properties shown in Figure 3 are used. DHC analysis is performed by an in-house axisymmetric thermal FE code. The FE mesh and its dimensions are shown in Figure 4 and Table 1. The FE model comprises 4 node isoparametric quadrilateral elements, and the back surface is assumed to be adiabatic.

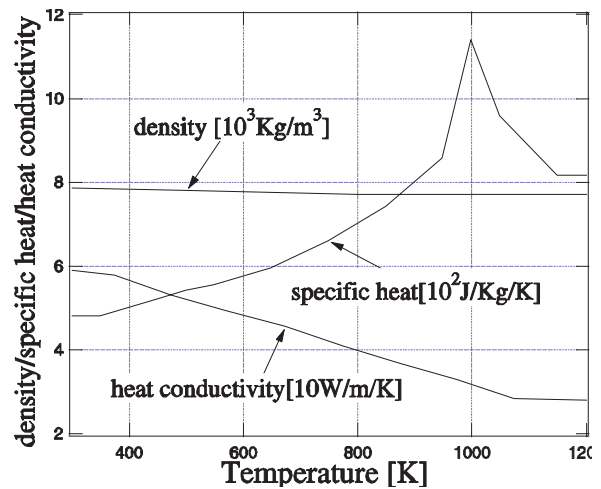


Figure 3: Temperature dependency of the thermal material properties



Figure 4: Axisymmetric FE mesh used in DHC analysis

The initial temperature is 300K. The convective heat transfer between plate and air is evaluated at the outer end, and its coefficient is 480 W/(m<sup>2</sup>K). In time integration, iterative calculation by Newman's method is repeated till the residual temperature norm becomes less than  $10^{-6}$  times as much as the nodal temperature norm. The numerical damping is 0.01, and the time increment is in the region of  $10^{-4} \sim 5 \times 10^{-2}$  sec.

The coefficients  $Q_k$  of Eq. (2) at time  $t_i$ ,  $Q_k^i$  are identified by Eq. (3). Heat flux distribution at

Table 1: Model dimensions of the FE mesh for DHC analysis of the spot heating tests

Model dimensions	$0.3 \times 0.006$ (m)
Num. of Elements	$40 \times 40 \times 6$
Max./Min. element size in $x$ dir	$3.44/13.8 (\times 10^{-3})$ m
Max./Min. element size in $y$ dir	$3.44/13.8 (\times 10^{-3})$ m
Max./Min. element size in $z$ dir	$5.04/16.8 (\times 10^{-4})$ m

time  $t_i$ ,  $q(t_i; r)$ , is given by substituting these coefficients into Eq. (2). Heating face temperature distribution at time  $t_i$ ,  $T_S(t_i; r)$ , is calculated by DHC analysis using the identified  $q(t_i; r)$  as a thermal boundary condition.

Figure 5 and Figure 6 show the identified distributions of flux  $q(t_i; r)$  and plate face temperature  $T_S(t_i; r)$  at time  $t=0.5, 1.0, 1.5, 2.0$  and  $2.5$  sec. It is found that instability is well controlled, and  $q$  and  $T_S$  are the highest at the center.  $q$  decreases and  $T_S$  increases with time, except at time  $t=0.5$ sec, at which point the thermal-flow field is in a transient state.

Figure 7 shows the relationship between  $q$  and  $T_S$  obtained by the regularized analysis. According to Eq. (1),  $q$  decreases as  $T_S$  rises, and a linear relationship is established between them. Figure 7 shows that such linear relationship is established after approximately  $t=1.5$ sec.

The result obtained supports the hypothesis (outlined in the previous section) that the entire heat transmission can be treated as heat transfer, and the overall local heat transfer coefficient,  $\alpha$ , remains unchanged with time.

### 3.4 Identification of the heat input parameters

The time-independent heat input parameters, the temperature of the gas adjacent to the plate  $T_G$  and local overall heat coefficient  $\alpha$ , can be identified by performing a linear regression analysis on the relation between  $q(t; r)$  and  $T_S(t; r)$  using Eq. (1).

There is no steep temperature gradient in the vertical direction in the vicinity of the bottom end of the LIF measurement region (0.5 mm above the

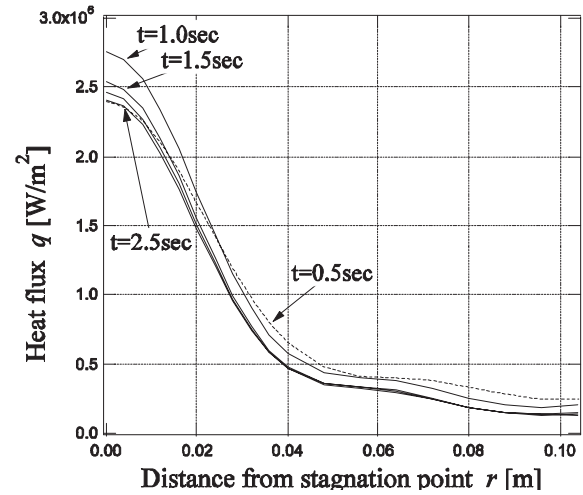


Figure 5: Distributions of heat flux identified by an inverse heat conduction analysis

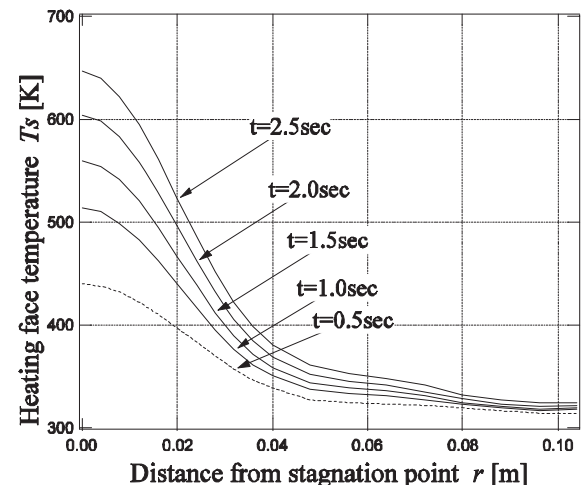


Figure 6: Distributions of plate face temperature identified by an inverse heat conduction analysis

plate face). This indicates that this region is on the outer side of the boundary layer, and that the gas temperature at the bottom end is almost equal to the temperature at the point adjacent to the boundary layer,  $T_G$ .

Figure 8 shows the distributions of the identified and measured  $T_G$ . The measured  $T_G$  is the gas temperature on the bottom end of the LIF measurement region, and the identified  $T_G$  proves to be largely in agreement with the measured one.

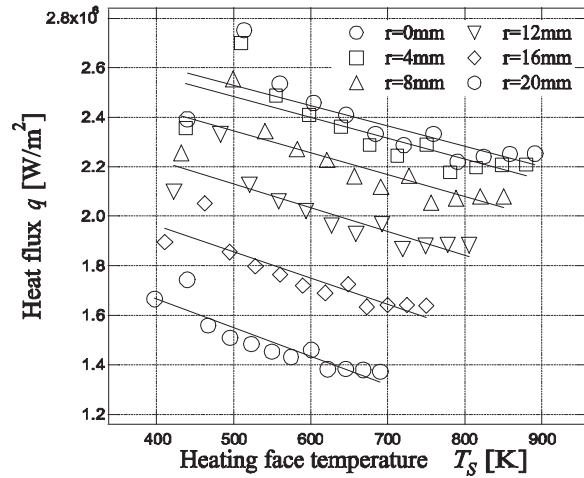


Figure 7: Relationship between heat flux and plate heating face temperature at various points on the plate

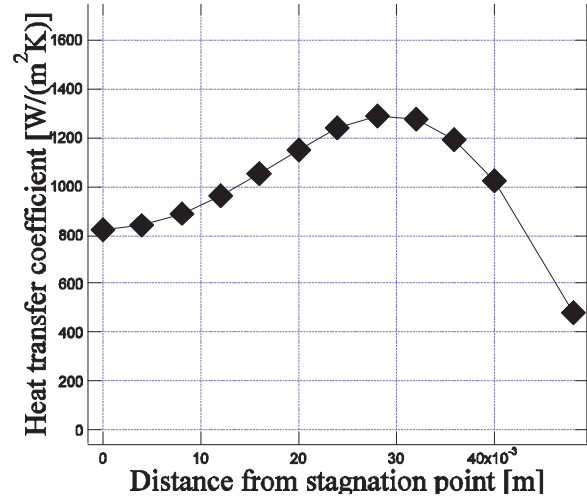


Figure 9: Distribution of the estimated local over-all heat transfer coefficient  $\alpha$

The identified distribution of  $\alpha$  is shown in Figure 9.

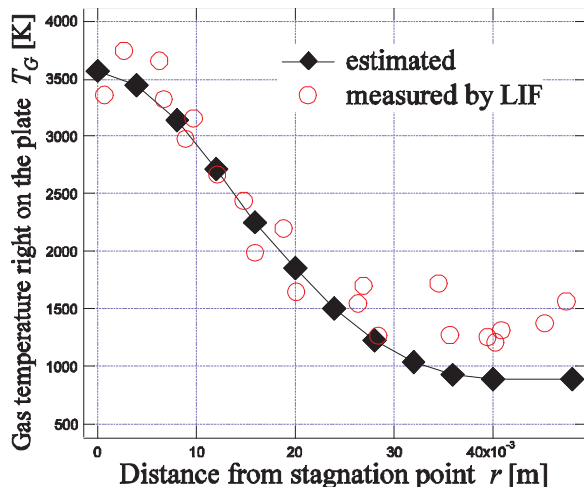


Figure 8: Distribution of the identified and measured gas temperature right on the plate  $T_G$

The time history of the back surface temperature can be calculated by DHC analysis using the identified  $T_G$  and  $\alpha$  as the thermal boundary conditions. The accuracy of the identified parameters can be investigated by comparing these calculated and measured back surface temperatures. The FE analysis is performed by the FE code used in the IHC analysis of the previous section. This code

has the capability to automatically generate the heat transfer boundary conditions on the heating face from the distributions of the heat input parameters. The material properties shown in Figure 3 and FE mesh shown in Figure 4 are employed, and the calculation conditions are the same as those for IHC analysis. Figure 10 compares the measured and calculated back surface temperatures, which coincide well.

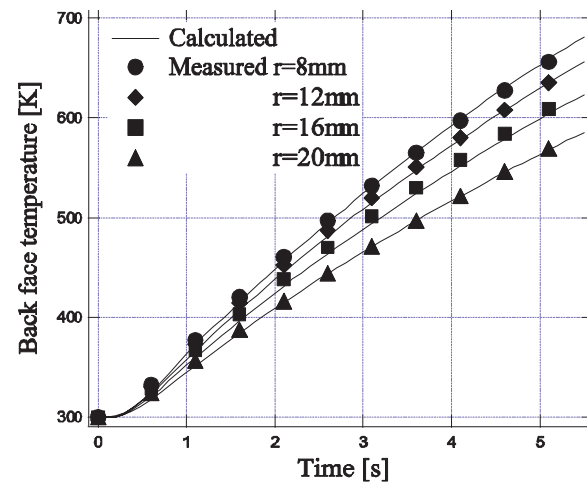


Figure 10: Comparison of the measured plate back surface temperatures during spot heating test with the ones obtained by direct heat conduction analysis using the identified  $T_G$  and  $\alpha$ .

The results obtained demonstrate the accuracy of the identified heat input parameters, and the validity of the hypotheses on heat transmission between flame and plate.

#### 4 Plate Temperature Estimation during Line Heating Process

##### 4.1 *Changing nature of the thermal-flow field in combustion flame during line heating process*

Deguchi, Yamaura, Tomita, Osawa, Hashimoto, Shinkai, Sawamura and Sugiyama (2002) measured the transient temperature field of the gas flame during a line heating test using a LIF system. They showed that the relative distribution of gas temperature around the moving torch is almost the same as that of the spot heating test under the same gas conditions. They also showed that this relative distribution is almost unchanged regardless of the temperature increase of the plate face. These results lead to the assumption that the relative distributions of  $T_G$  and  $\alpha$  around the torch during the line heating process can be approximated as time independent and nearly the same as those of the spot heating test under the same gas conditions.

According to this hypothesis, the heat transmission during a line heating test can be calculated with sufficient precision when we repeatedly analyze heat transfer and heat conduction over very short durations using  $T_G$  and  $\alpha$  of the spot heating test. In this new plate temperature estimation method, the change in the plate temperature is automatically taken into account in the context of heat transfer analysis. The validity of this proposed method has been investigated by comparing the measured and calculated plate temperature during line heating experiments.

##### 4.2 *Line heating test*

A rectangular steel plate, as shown in Figure 11, with length 200mm, width 160mm and thickness 16mm, is arranged horizontally and a torch is positioned above the plate. Gas heating is carried out by moving along the center line of the plate at a constant speed with a traverse mechanism. The

torch speed  $V$  is chosen as  $V=10.22$  mm/sec., and the plate is heated by an oxypropane flame. The torch height, the nozzle, the pressure and the flux of propane and oxygen are chosen so that they are the same as those of the spot heating test.

K-type thermocouples with a sheath diameter of 0.32mm are placed at 4 locations, as shown in Figure 11. The distance between the heating face and the thermocouple is 2.5mm, and the transversal distance from the center line  $\eta$  is 0, 20, 40 and 60 mm. Thermocouple outputs are recorded in a personal computer every 0.5sec., and the internal temperature of the steel plate is about 300K.

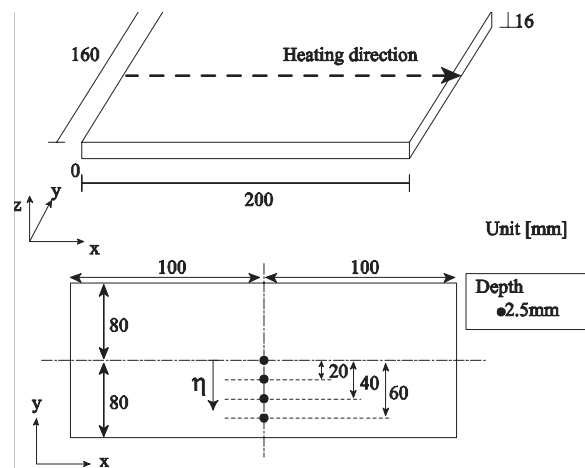


Figure 11: Rectangular steel plate used in the line heating test

##### 4.3 *Direct heat conduction analysis of the line heating test*

Direct heat conduction analysis is performed by an in-house 3-dimensional thermal FE code. This code has the capability to automatically generate the heat transfer boundary conditions around the moving torch from the heat input parameters,  $T_G$  and  $\alpha$ . The FE mesh and its dimensions are shown in Figure 12 and Table 2. This FE model comprises 8 node isoparametric hexahedron elements, and the convective heat transfer between plate and air is evaluated at the back surface and the outer sides. The temperature dependencies of the material properties shown in Figure 3 are used, and the initial temperature is set to 300K. Other

calculation parameters are equal to those of the direct analysis of the spot heating test.

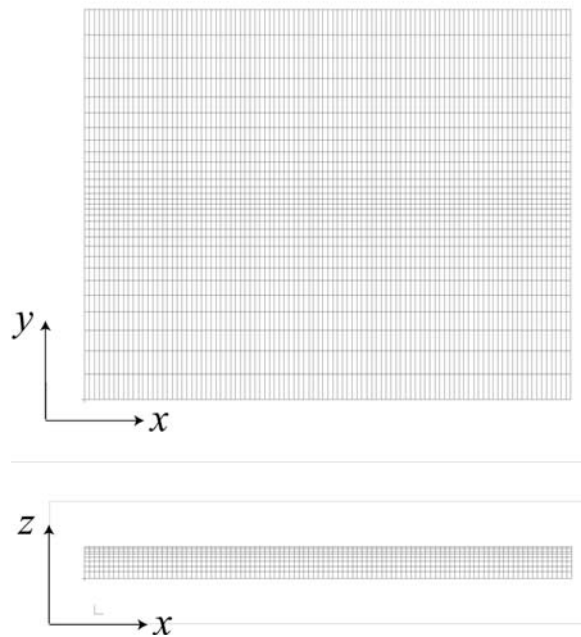


Figure 12: FE mesh of the rectangular plate used in the direct heat conduction analysis of the line heating test

Table 2: Model dimensions of the FE model for the direct heat conduction analysis of the line heating test

Model dimensions	$0.2 \times 0.16 \times 0.016$ (m)
Num. of Elements	$100 \times 30 \times 8$
Max./Min. element size in $x$ dir	$2.00/2.00 (\times 10^{-3})$ m
Max./Min. element size in $y$ dir	$2.11/10.6 (\times 10^{-3})$ m
Max./Min. element size in $z$ dir	$13.2/44.0 (\times 10^{-4})$ m

Figure 13 compares the calculated and plate temperatures measured during the line heating test, which closely agree. The estimation error is at its maximum at the point where  $\eta=0$ , and the error is less than 30K. The accuracy of estimated temperatures with the proposed method compares favorably with that of conventional studies (e.g.,

Yu, Anderson, Maekawa and Patrikalakis (2001)). The insufficient accuracy of the thermal material properties, especially in the high temperature region, is the conceivable cause of any calculation error.

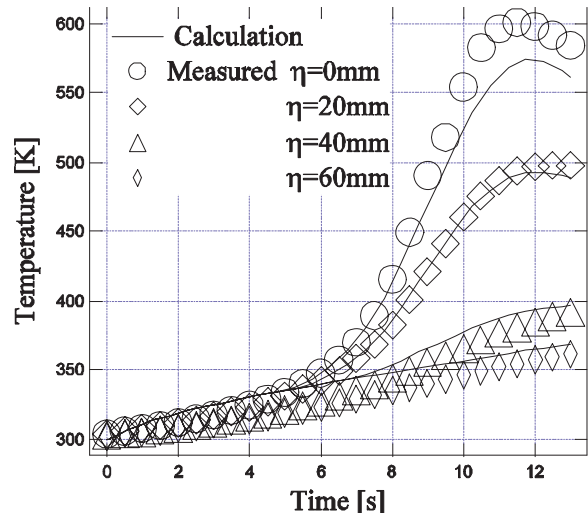


Figure 13: Comparison of the measured plate temperatures during the line heating test with the ones obtained by direct heat conduction analysis using the identified TG and in the spot heating test

In this line heating case, the calculated plate temperature immediately below the torch becomes constant in a short time, and remains unchanged with time. In contrast, the heating face temperature increases with time in the spot heating test, as shown in Figure 6. Plate temperature during the spot and line heating tests can be estimated with sufficient precision solely from the heat input parameters identified by the spot heating test.

This indicates that accurate estimates of plate temperature can be made regardless of the change in the plate heating face temperature. The proposed method for estimating temperatures is therefore valid for any desired torch movement history. It is felt that this new method is applicable to slow torch speed and repetitive heating situations.

## 5 Conclusions

A new hypothesis on heat transmission during line heating has been proposed. It states that the dis-

tribution of the temperature of the gas adjacent to the plate,  $T_G$ , and local overall heat transfer coefficient  $\alpha$  depend only on the distance from the torch. An identification technique for  $T_G$  and  $\alpha$  has been developed, and the validity of the employed hypothesis and the proposed technique were investigated by comparing the measured and identified  $T_G$  during a spot heating test.

The main results are as follows:

- Distributions of  $T_G$  and  $\alpha$  during a spot heating test can be identified by IHC analysis. The identified  $T_G$  is close to the one measured by a LIF system.
- The plate back surface temperature during the spot heating test calculated from the identified  $T_G$  and  $\alpha$  is comparable to the one measured. The results obtained demonstrate the accuracy of the identified heat input parameters and the validity of the hypothesis on heat transmission.
- The plate temperature during the line heating test calculated from  $T_G$  and  $\alpha$  of the spot heating test also coincides with the one measured. This indicates that accurate estimates of plate temperature can be made regardless of the change in the plate heating face temperature solely from the spot heating test results.

**Acknowledgement:** Part of this study was supported by Fundamental Research Developing Association for Shipbuilding and Offshore, Japan, and appreciation is extended to all those associated with the program and the award.

## References

**Beck, J.V.; Blackwell, B. and Clair, C.R.S.T.** (1985): *Inverse Heat Conduction*, Wiley-Interscience.

**Chang, C.W.; Liu, C.S. and Chang, J.R.** (2005): A Group Preserving Scheme for Inverse Heat Conduction Problems. *CMES: Computer Modeling in Engineering & Sciences*, 10, 1, pp.13-38.

**Deguchi, Y.; Nakagawa, H.; Ichinose, T. and Inada, M.** (2000): LIF Applications for Practical Combustors. *Journal of Visualization*, 2, 3/4, pp.343-352.

**Deguchi, Y.; Yamaura, T.; Tomita, Y.; Osawa, N.; Hashimoto, K.; Shinkai, N.; Sawamura, J. and Sugiyama K.** (2002): A Study on Heat Transfer to Steel Plate from Combustion Flux in Line Heating. *Proc. 10th Int. Symposium on Flow Visualization*, Paper F0163.

**Eckbreth, A.C.** (1988): *Laser Diagnostics for Combustion Temperature and Species*, ABACUS Press.

**Jang C.D.; Seo, S.I. and Ko, D.E.** (1997): A Study on the Prediction of Deformation of Plates Due to Line Heating Using a Simplified Thermal Elasto-Plastic Analysis. *Journal of Ship Production*, 13, 1, pp. 22-27.

**Ling, X. and Atluri, S.N.** (2006): Stability Analysis for Inverse Heat Conduction Problems. *CMES: Computer Modeling in Engineering & Sciences*, 13, 3, pp.219-228.

**Liu, C.S.** (2006): An Efficient Simultaneous Estimation of Temperature-Dependent Thermophysical Properties. *CMES: Computer Modeling in Engineering & Sciences*, 14, 2, pp.77-90.

**Liu, C.S.; Liu L.W. and Hong, H.K.** (2007): Highly Accurate Computation of Spatial-Dependent Heat Conductivity and Heat Capacity in Inverse Thermal Problem. *CMES: Computer Modeling in Engineering & Sciences*, 17, 1, pp.1-18.

**Moshaiov, A. and Latorre, R.** (1985): Temperature Distribution During Plate Bending by Torch Flame Heating. *Journal of Ship Research*, 29, 1, pp.1-11.

**Reisel, J.R.; Carter, C.D. and Laurendeau, N.M.** (1992): Einstein Coefficients for Rotational Lines of the (0,0) Band of the  $\text{NO } A^2\Sigma^+ - X^2\Pi$  System. *Journal of Quantitative Spectroscopy and Radiative Transfer*, 47, 1, pp. 43-54.

**Sawamura, J.; Tomita, Y.; Osawa, N. and Hashimoto, K.** (2002): Study on Combustion Analysis in the Impinging Jet Flame during Line Heating Process, *Proc. 12th International Offshore and Polar Engineering Conference*, IV, pp.

247-252.

**Shin, J.G. and Woo, J.H.** (2003): Analysis of Heat Transfer Between the Gas Torch and the Plate For the Application of Line Heating. *Journal of Manufacturing Science and Engineering*, 125, 4, pp. 794-800.

**Terasaki, T.; Kitamura, N. and Nakai, M.** (1999): Predictive Equation for Thermal Cycle Generated by Line Heating Method. *Trans. The West-Japan Soc. Naval Architects*, 99, pp.321-329 (in Japanese).

**Tsuji, I. and Okumura Y.** (1988): A Study on Line Heating Process for Plate Bending of Ship Steels. *Trans. The West-Japan Soc. Naval Architects*, 76, pp.149-160 (in Japanese).

**Tomita, Y.; Osawa, N.; Hashimoto, K.; Shinkai, N.; Sawamura, J. and Matsuoka, K.** (2001): Study on Heat Transfer between Gas Flame and Plate during Line-Heating Process. In: Y.S. Wu, W.C. Cui and G.J. Zhou (ed) *Practical Design of Ships and Other Floating Structures*, Elsevier, pp. 389-396.

**Yu, G.; Anderson, R.J.; Maekawa, T. and Patrikalakis, N.M.** (2001): Efficient Simulation of Shell Forming by Line Heating. *International Journal of Mechanical Sciences*, 43, pp.2349-2370.

